

On cosmic ray acceleration in supernova remnants and the FERMI/PAMELA data

Markus Ahlers, Philipp Mertsch, and Subir Sarkar

Rudolf Peierls Centre for Theoretical Physics, University of Oxford, Oxford OX1 3NP, UK

We discuss recent observations of high energy cosmic ray positrons and electrons in the context of hadronic interactions in supernova remnants, the suspected accelerators of galactic cosmic rays. Diffusive shock acceleration can harden the energy spectrum of secondary positrons relative to that of the primary protons and electrons and thus explain the rise in the positron fraction observed by PAMELA above 10 GeV. We normalize the hadronic interaction rate by holding pion decay to be responsible for the gamma-rays detected by HESS from some SNRs. By simulating the spatial and temporal distribution of SNRs in the Galaxy according to their known statistics, we are able to then fit the electron (plus positron) energy spectrum measured by Fermi. It appears that IceCube has good prospects for detecting the hadronic neutrino fluxes expected from nearby SNRs.

PACS numbers: 98.70.Sa, 96.50.sb, 98.58.Mj

I. INTRODUCTION

Recently, the PAMELA collaboration has published data on the positron fraction, $J_{e^+}/(J_{e^-} + J_{e^+})$, in galactic cosmic rays (GCR) which is seen to *increase* between ~ 10 and 100 GeV [1], in contrast to the prediction of the standard GCR propagation model [2]. The model assumes that the positrons are secondaries created via interactions of GCR protons and nuclei with interstellar matter, hence their spectrum should be softer than that of primary electrons and the positron fraction should thus decrease with energy [3]. The combined differential flux of GCR electrons and positrons, $(J_{e^-} + J_{e^+})$, has also been measured with the Fermi Large Area Telescope (LAT) and is approximately fitted by a E^{-3} power-law in energy up to ~ 1 TeV [4]. Measurements by the HESS collaboration [5, 6] show significant steepening of the spectrum beyond ~ 1 TeV, while agreeing well with the Fermi data at lower energies. Although the Fermi LAT data does not confirm the sharp feature claimed earlier by the ATIC collaboration [7], there does appear to be a small excess flux above ~ 100 GeV in comparison with standard GCR propagation models [2, 8].

Both these experimental findings have generated a lot of interest because they may be an indirect signature of dark matter particles. Annihilation or decay of galactic dark matter can produce electrons and positrons with a spectrum considerably harder than that of primary electrons. Besides the fine-tuning challenges such models face [8, 9], other cosmic ray data provide important constraints. The antiproton-to-proton ratio observed by PAMELA [10] is in good agreement with the prediction of secondary production by GCRs and thus rules out most dark matter annihilation/decay models which have hadronic final states. Even purely leptonic annihilation channels are strongly constrained by the Galactic synchrotron radio background [11] and by the Galactic gamma-ray background [12]. In fact pulsars may produce a hard spectrum of electron-positron pairs in the right energy range to explain both the positron flux anomaly and the observed electron flux [13, 14].

It has long been believed [15] that GCRs are generated by diffusive shock acceleration (DSA) [16, 17] in supernova remnants (SNRs) [18]. Hadronic interactions of the accelerated protons will create π^\pm (and π^0) which then decay to yield secondary e^\pm and neutrinos (and γ -rays). It has been suggested that the *acceleration* of the secondary positrons in a nearby SNR shock wave may be responsible for the PAMELA anomaly [19]. The fraction of secondary e^+ which are accelerated increases with energy, so their final spectrum is *harder* than the injected spectrum. This effect had been noted earlier as a general expectation for the secondary-to-primary ratio in the presence of stochastic Fermi acceleration [20, 21]. A similar effect is then predicted at higher energies for both antiprotons [22, 23] and for secondary nuclei such as boron [24]. These predictions will be tested soon with data from PAMELA and the forthcoming AMS-02 mission [25].

It is interesting to ask whether this model can account also for the absolute fluxes of e^- (and e^+) in GCR at energies $\gtrsim 100$ GeV [19]. This is rather sensitive to the assumed spatial distribution of the sources so in this paper we consider a realistic distribution of SNRs based on astronomical data (Sec. II). Previously the flux of secondary e^- and e^+ in the sources has been normalized with respect to the primary electrons in an *ad hoc* fashion [19]. Instead, we exploit the hadronic origin of these secondaries and normalize using the γ -ray fluxes (assumed to be from π^0 decay) detected from known SNRs by HESS. We can thus fix the only free model parameter by fitting the total $e^- + e^+$ flux to Fermi LAT and HESS data (Sec. III). The e^+ fraction is then *predicted* up to TeV energies and provides a good match to PAMELA data (Sec. IV). Having constrained the distribution of the closest SNRs via the measured e^- and e^+ spectra, we present an example of a likely source distribution in order to illustrate that there are good prospects for IceCube to detect neutrinos from nearby SNR. A consistent picture thus emerges for all presently available data in the framework of the standard DSA/SNR origin model of GCR. However there remain some open issues and grounds for concern which we discuss at the end (Sec. V).

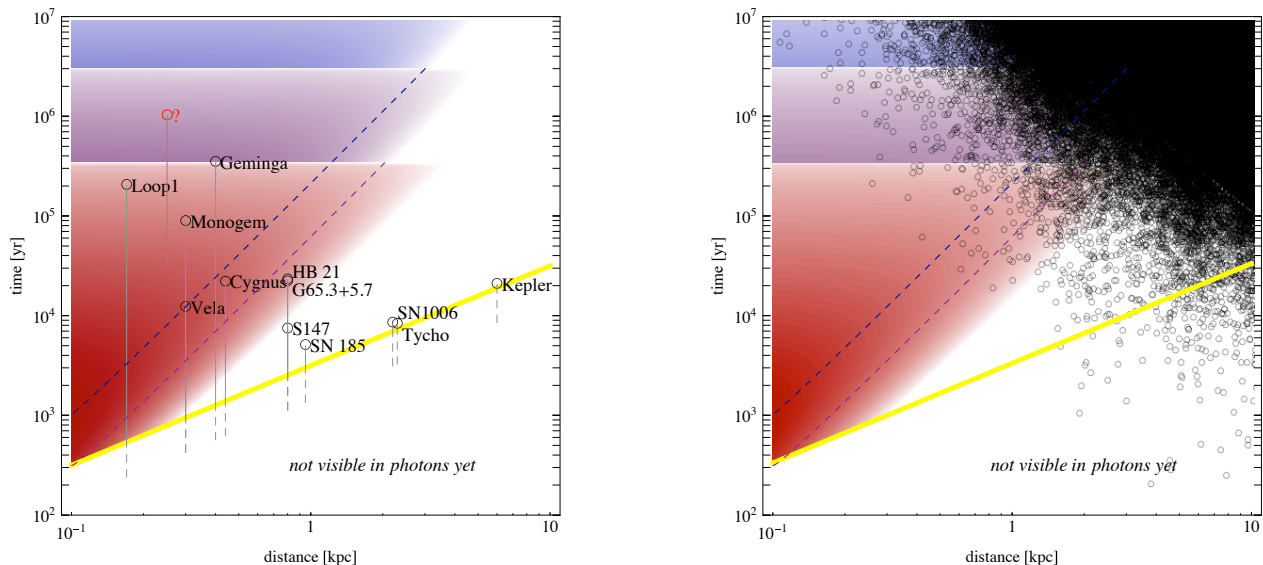


FIG. 1: Distance-time diagram for nearby SNRs (after Ref. [30]). **Left:** The open circles mark supernova events and the world-lines of the discovered remnants are indicated. The thick yellow line is our past light-cone; all events lying on it, *e.g.*, the SNR world-lines touching it, can be observed presently. The blue, purple and red shadings (top to bottom) show the relative contribution of sources to the diffuse e^- and e^+ flux observed at Earth at 10, 100 and 1000 GeV, respectively. The open red circle is an example of a hypothetical supernova whose remnant is too old to be visible any longer but which might still be contributing to the diffuse e^- and e^+ flux. **Right:** A distance-time diagram for hypothetical nearby SNRs. The open black circles are an example of a possible “history” of supernovae (the worldlines have been suppressed) as simulated by our Monte Carlo calculation (see Section II).

II. DIFFUSION MODEL AND SOURCE DISTRIBUTION

The diffusive transport of high energy e^- and e^+ in the Galaxy is governed by the equation [15],

$$\frac{\partial n_{\pm}}{\partial t} = \nabla \cdot (D_{\text{GCR}} \nabla n_{\pm}) + \frac{\partial}{\partial E} (bn_{\pm}) + Q_{\pm}, \quad (1)$$

where $n_{\pm} dE \equiv n_{\pm}(r, t, E) dE$ denotes the particle density of e^+ and e^- with energy in $[E, E + dE]$. The spatial diffusion coefficient is assumed not to depend on the position in the Galaxy but only on energy: $D_{\text{GCR}}(E) = D_0 E^{\delta}$. The energy loss rate of GCR e^- and e^+ through synchrotron radiation in Galactic magnetic fields and inverse Compton scattering on the CMB and interstellar radiation backgrounds is parametrized as $b(E) = b_0 E^2$. Finally, Q_{\pm} denotes the injection of electrons and positrons from both (possible) primary and secondary sources. In the majority of previous calculations, in particular the GALPROP code [2] in its conventional setup, the distribution of sources is assumed to be continuous. However at energies when the diffusion length ℓ becomes smaller than the distance to the closest source (similar to the average distance between sources for a homogeneous distribution) the fact that the sources are discrete should become important. This effect on GCR electrons was first pointed out in Ref. [26] and has later been considered in more detail [27, 28, 29]. It has also been studied using an extended version of GALPROP [30].

Assuming that all the electrons and positrons are released instantly at the end of the Sedov-Taylor phase of expansion when the SNR becomes radiative, the flux of N sources at distances r_i and times t_i is given by the sum over the corresponding Green’s functions (see Appendix A) for the particle density (times the usual “flux factor”, $c/4\pi$, for an isotropic population of relativistic particles):

$$J_N(E) = \frac{c}{4\pi} \sum_{i=1}^N G_{\text{disk}}(E, r_i, t_i). \quad (2)$$

The spatial distribution and temporal history of GCR sources, $\{r_i, t_i\}$, is not known *a priori* but can be modelled for an assumed source class *e.g.*, SNRs. At low energies, the GCR diffusion length is long enough such that the approximation of a continuous source density is acceptable. For energies above some hundreds of GeV, however, the fluctuations introduced by the discreteness of the sources cannot be neglected any longer.

Some authors [28, 31] have assumed a continuous distribution of sources for distances beyond a few hundred parsecs, supplemented by a set of known SNRs for smaller distances. This approach is however biased by the choice of young, nearby sources which have been detected in radio and/or X-rays. Older sources may not be visible in photons any longer but still be contributing to the GCR electron flux, see Fig. 1. We note that the effect of this incomplete assumed source distribution is a dip in the electron flux seen in both analyses [28, 31], although at

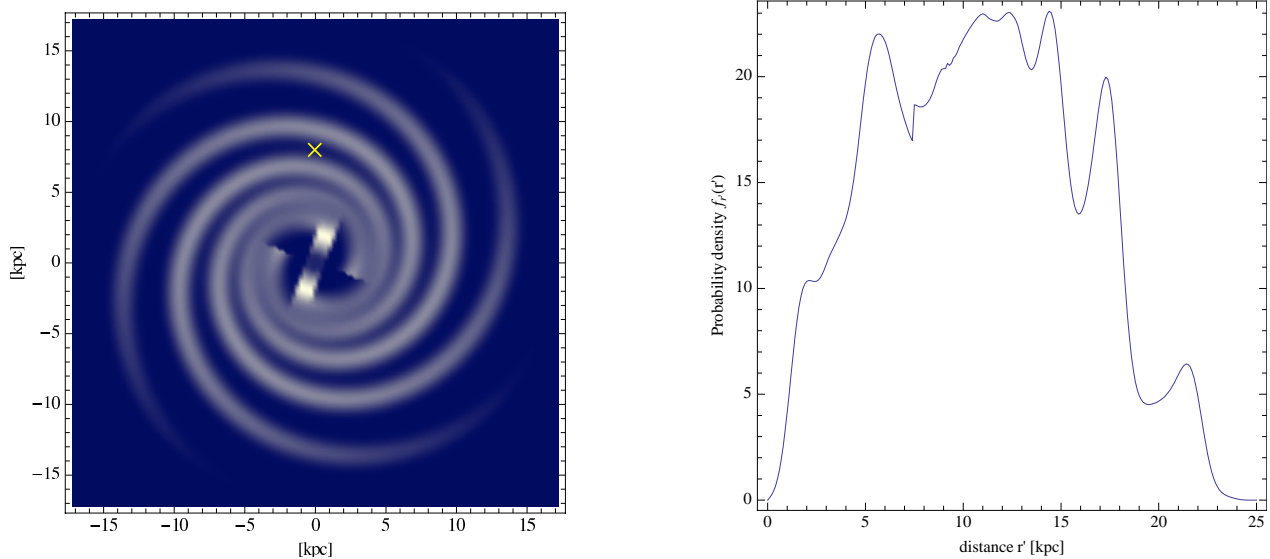


FIG. 2: **Left:** The assumed distribution of SNRs in the Galaxy; the cross denotes the position of the Sun in between two spiral arms. **Right:** The probability density for the distance of a SNR from the Sun.

different energies because of the different diffusion model parameters chosen.

Determining the complete distribution of sources in our vicinity (*i.e.* up to a few kpc) from observations seems challenging. However it turns out that we do not need to know the exact distribution in order to calculate the e^+ flux but require only a limited amount of information, most of which is encoded already in the dominant e^- flux. By including the recent measurements by Fermi LAT [4] and HESS [5, 6] of the total $e^- + e^+$ flux in the energy region of interest, we have sufficient information at hand to make a prediction for the positron fraction under the assumption that the additional positrons originate in the same sources.

We perform a Monte Carlo calculation by considering a large number of random distributions of sources drawn from a probability density function that reflects our astronomical knowledge about the distribution of SNRs in the Galaxy. The better the flux of e^- and e^+ from such a “history” of sources reproduces the measured fluxes, the closer is the underlying distribution of sources likely to be to the actual one. Of course all SNRs are not the same, however variations of the source parameters would only introduce additional fluctuations into the fluxes without altering their average. We can choose the best “fit” to the data and thus determine the e^+ flux.

The smoothed radial distribution of SNRs in the Galaxy is well modelled by [32]:

$$f(r) = A \sin\left(\frac{\pi r}{r_0} + \theta_0\right) e^{-\beta r}, \quad (3)$$

where $A = 1.96 \text{ kpc}^{-2}$, $r_0 = 17.2 \text{ kpc}$, $\theta_0 = 0.08$ and $\beta = 0.13$. To obtain a realistic probability density for the distance between the Earth and a SNR we have to also take into account the spiral structure of the Galaxy.

We adopt a logarithmic spiral with four arms of pitch angle 12.6° and a central bar of 6 kpc length inclined by 30° with respect to the direction Sun - Galactic centre [33]. The density of SNRs is modelled by a Gaussian with 500 pc dispersion for each arm [27]. The resulting distribution $g(r, \phi)$ (see left panel of Fig. 2) has been normalized with respect to azimuth in such a way that the above radial distribution (3) is recovered. To obtain the probability density for the distances we transform to the coordinates (r', ϕ') centered on the Sun. As the e^- and e^+ fluxes are assumed to be isotropic, we can average over the polar angle ϕ' , such that the probability density $f_{r'}(r')$ depends only on the distance r' to the source,

$$f_{r'}(r') = \frac{1}{2\pi} \int_0^{2\pi} d\phi' r' g(r', \phi', \phi(r', \phi')). \quad (4)$$

This function is shown in the right panel of Fig. 2.

We assume that the sources are uniformly distributed in time, *i.e.* their probability density $f_t(t)$ is

$$f_t(t) = \begin{cases} 1/t_{\max} & \text{for } 0 \leq t \leq t_{\max}, \\ 0 & \text{otherwise,} \end{cases} \quad (5)$$

with t_{\max} standing for the earliest time considered, which is related to the minimum energy for which our calculation is valid through:

$$t_{\max} = (bE_{\min})^{-1}. \quad (6)$$

The total number N of sources that are needed in the Monte Carlo to reproduce the (observed) number $\mathcal{N} \simeq 300$ of SNRs active in the galaxy at any given time depends on the average lifetime of a SNR, τ_{SNR} , which is suggested to be $\sim 10^4 \text{ yr}$ [18], hence

$$N = 3 \times 10^6 \left(\frac{\mathcal{N}}{300}\right) \left(\frac{t_{\max}}{10^8 \text{ yr}}\right) \left(\frac{\tau_{\text{SNR}}}{10^4 \text{ yr}}\right)^{-1}. \quad (7)$$

Source	Other name(s)	Γ	$J_\gamma^0 \div 10^{-12}$ [(cm ² s TeV) ⁻¹]	E_{\max} [TeV]	d [kpc]	$Q_\gamma^0 \div 10^{33}$ [(s TeV) ⁻¹]	Ref.
HESS J0852–463	RX J0852.0-4622 (Vela Junior)	2.1 ± 0.1	21 ± 2	> 10	0.2	0.10	[34]
HESS J1442–624	RCW 86, SN 185 (?)	2.54 ± 0.12	3.72 ± 0.50	$\gtrsim 20$	1	0.46	[35]
HESS J1713–381	CTB 37B, G348.7+0.3	2.65 ± 0.19	0.65 ± 0.11	$\gtrsim 15$	7	3.812	[36]
HESS J1713–397	RX J1713.7-3946, G347.3-0.5	2.04 ± 0.04	21.3 ± 0.5	17.9 ± 3.3	1	2.55	[37, 38]
HESS J1714–385	CTB 37A	2.30 ± 0.13	0.87 ± 0.1	$\gtrsim 12$	11.3	13.3	[39]
HESS J1731–347	G 353.6-07	2.26 ± 0.10	6.1 ± 0.8	$\gtrsim 80$	3.2	7.48	[40, 41]
HESS J1801–233 ^a	W 28, GRO J1801-2320	2.66 ± 0.27	0.75 ± 0.11	$\gtrsim 4$	2	0.359	[42]
HESS J1804–216 ^b	W 30, G8.7-0.1	2.72 ± 0.06	5.74	$\gtrsim 10$	6	24.73	[44]
HESS J1834–087	W 41, G23.3-0.3	2.45 ± 0.16	2.63	$\gtrsim 3$	5	7.87	[44]
MAGIC J0616+225	IC 443	3.1 ± 0.3	0.58	$\gtrsim 1$	1.5	0.156	[45]
Cassiopeia A		2.4 ± 0.2	1.0 ± 0.1	$\gtrsim 40$	3.4	1.38	[46] ^c
J0632+057	Monoceros	2.53 ± 0.26	0.91 ± 0.17	N/A	1.6	0.279	[48]
Mean		~ 2.5		$\gtrsim 20$		~ 5.2	
Mean, excluding sources with $\Gamma > 2.8$		~ 2.4		$\gtrsim 20$		~ 5.7	
Mean, excluding sources with $\Gamma > 2.6$		~ 2.3		$\gtrsim 20$		~ 4.2	

^aWe assume that W 28 powers only the emission from J1801–233 (and not the nearby J1800–240 A, B and C).

^bW30 is taken to be the origin of the VHE emission [43].

^cCas A was first detected by HEGRA [47].

TABLE I: Summary of spectral parameters for SNRs detected in γ -rays from a power-law fit to the spectrum, $J_\gamma = J_\gamma^0 (E/\text{TeV})^{-\Gamma}$, with an exponential cut-off at E_{\max} in the case of HESS J1713.7-397. The errors shown are statistical only — the systematic error is conservatively estimated to be 20% on the flux J_γ and ± 0.2 on the spectral index Γ . Also shown is the estimated distance d and the injection rate Q_γ^0 derived from Eq. (24).

III. FITTING THE $e^+ + e^-$ SPECTRA

A schematic description of the present framework is shown in Fig. 3. Cosmic rays are shock accelerated in SNRs and then diffuse through the Galaxy to Earth undergoing collisions with interstellar matter *en route* and creating secondary e^+ . As discussed, the ratio of the secondary e^+ to the primary e^- from the sources should *decrease* with energy, in contrast to the behaviour seen by PAMELA. We follow Ref. [19] in explaining this by invoking a new component of e^+ which is produced through cosmic ray interactions in the SNRs, and then shock *accelerated*, thus yielding a harder spectrum than that of their primaries. We discuss these components in turn below and calculate their relative contributions by normalising to the γ -ray flux from the SNRs, which provides an independent measure of the hadronic interactions therein.

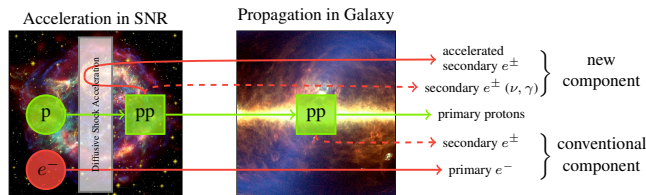


FIG. 3: Schematic description of contributions to the galactic cosmic rays observed at Earth in the present framework.

A. Primary electrons

The radio and X-ray emission observed from SNRs is interpreted as synchrotron radiation of electrons accelerated up to energies of $\mathcal{O}(100)$ TeV [18]. The spectrum of this radiation then determines the spectrum of the underlying relativistic electrons. Moreover the theory of diffusive shock acceleration [16, 17] predicts similar spectra for the accelerated protons and nuclei as for the electrons. If the γ -ray emission observed by HESS from a number of identified SNRs is assumed to be of hadronic origin, we can use the measured spectra to constrain both the relativistic proton and electron population.

Table I shows a compilation of γ -ray sources observed by HESS that have been identified as SNRs. We have included all identified shell-type SNRs and strong SNR candidates in the HESS source catalogue [49], and also added the SNRs IC 443, Cassiopeia A and Monoceros. Actually it is not clear that the acceleration of secondaries does occur in all the SNRs considered, especially when the γ -ray emission is associated with a neighbouring molecular cloud rather than coming from the vicinity of the shock wave. In fact the γ -rays could equally well be due to inverse-Compton scattering by the relativistic electrons responsible for the observed synchrotron radio and X-ray emission. Therefore, we have considered three possibilities — including all sources implies a mean power-law spectral index for the protons of $\langle \Gamma \rangle = 2.5$, while excluding steep spectrum sources with $\Gamma > 2.8$ gives $\langle \Gamma \rangle = 2.3$

and excluding sources with $\Gamma > 2.6$ yields $\langle \Gamma \rangle = 2.4$. In the following we adopt the central value, $\Gamma = 2.4$, for the electron population too, unless stated otherwise. This requires a compression factor of $r \leq 3.3$ in contrast to the value of $r = 4$ expected for a strong shock, so there is clearly some tension between the DSA theory and observations. This can possibly be resolved if we consider only a subset of the SNRs in Table 1 to be hadronic accelerators, or if the γ -ray spectrum is steepened e.g. by the onset of an exponential cutoff in the electron spectrum. Our model assumptions are intimately connected to the production of neutrinos, the detection of which will therefore provide an independent test as we discuss later. In this work we adopt a cut-off of $E_{\text{cut}} \simeq 20$ TeV which is consistent with DSA theory [18]. The source spectrum of primary electrons is then:

$$R_{e^-} = R_{e^-}^0 \left(\frac{E}{\text{GeV}} \right)^{-\Gamma} e^{-E/E_{\text{cut}}}. \quad (8)$$

The normalisation $R_{e^-}^0$ is determined by fitting the electron flux at Earth resulting from our Monte Carlo computation to the preliminary measurement by PAMELA at 10 GeV [50]; the secondary fluxes can be neglected for this normalisation. We find $R_{e^-}^0 = 1.8 \times 10^{50} \text{ GeV}^{-1}$ for $\Gamma = 2.4$ which corresponds to a total injection energy of

$$\int_{1 \text{ GeV}}^{20 \text{ TeV}} dE E R_{e^-}(E) \simeq 7 \times 10^{47} \text{ erg}. \quad (9)$$

This compares well to the value of 9.2×10^{47} erg said to be required to power the GCR electrons [18].

Solar modulation which is important below ~ 10 GeV, has been accounted for using the force field approach [51], with a charge-independent potential of $\phi = 600$ MV. However, our simple model ignores convection and (re)acceleration in the interstellar medium which become important below ~ 5 GeV, hence the electron flux cannot be predicted at lower energies. The primary e^- fluxes as measured on Earth for 30 different source configurations are shown in the top panel of Fig. 5. With an injection power-law index $\Gamma \simeq 2.4 \pm 0.1$ as required for consistency with the γ -ray data, there clearly is a deficit at high energies compared to the $e^+ + e^-$ flux measured by Fermi LAT and HESS.

B. Secondary electrons and positrons

Positrons in GCR are generally assumed to be of purely secondary origin, arising through the decay of pions and kaons produced in the interactions of GCR protons (and nuclei) with the interstellar medium (ISM) [2]. The neutral pions decay into γ -rays which then contribute to, if not dominantly constitute, the Galactic γ -ray background. The charged pions on the other hand decay into neutrinos and muons, the latter subsequently decaying into electrons and positrons. Assuming that spatial and

temporal variations in the GCR proton flux J_p and the ISM gas density n_{ISM} are small, the source density of these secondary background e^- and e^+ is also homogeneous, both in space and in time:

$$q_{\pm}^{\text{ISM}} = n_{\text{ISM}} c \int_{E_{\text{thr}}}^{\infty} dE' \frac{4\pi}{\beta c} J_p(E') \frac{d\sigma_{\text{pp} \rightarrow e^{\pm} + X}}{dE}, \quad (10)$$

where $d\sigma_{\text{pp} \rightarrow e^{\pm} + X}/dE$ is the partial differential cross-section for e^{\pm} production and $\beta \simeq 1$ is the velocity of the GCR. We can then integrate the Green's function for a single source over space and time to calculate

$$J_{\pm}(E) \simeq \frac{c}{4\pi |b(E)|} \int_E^{\infty} dE' q_{\pm}^{\text{ISM}}(E') \frac{2h}{\ell_{\text{cr}}} \chi \left(0, \frac{\ell}{\ell_{\text{cr}}} \right), \quad (11)$$

where χ and ℓ_{cr} are defined by Eq. (A2) of Appendix A, ℓ is the diffusion length defined by Eq. (A3), and $h \sim 0.1$ kpc is the height of the Galactic disk.

We calculate the flux of secondary background e^- and e^+ from the Solar-demodulated flux of GCR protons as derived from the BESS data [53] and model the cross-sections according to Ref. [54]. The contribution from kaon decay is subdominant and is therefore neglected. The presence of He both in GCRs and in the ISM is taken into account by multiplying the proton contribution by a factor of 1.2. Our results are in good agreement with Ref. [55], taking into account the different diffusion model parameters and keeping in mind that convection and reacceleration have been neglected here. These fluxes are shown (dashed line) in the middle panel of Fig. 5 and are clearly a subdominant component which cannot account for the deficit at high energies.

Moreover, the positron flux is *falling* at all energies whereas the PAMELA data [1] clearly show a *rise* above a few GeV. One way this can be resolved is if there is a dip in the electron spectrum between ~ 10 and 100 GeV. It has been suggested that Klein-Nishina corrections to the Thomson cross section for inverse Compton scattering [56] or inhomogeneities in the distribution of sources [31] can produce such a dip. However the former would require a rather enhanced interstellar background light (IBL) field [56], while the latter calculation [31] assumes an incomplete source distribution (see Sec. II) and moreover adopts diffusion model parameters quite different from those derived from the measured nuclear secondary-to-primary ratios [57] and the measured Galactic magnetic field and IBL [28].

The other, perhaps more straightforward possibility is to consider an additional component of GCR positrons with a *harder* source spectrum that results in a harder propagated spectrum and therefore leads to an increase in the positron fraction.

C. Secondary accelerated electrons and positrons

It has been suggested that *acceleration* of secondary e^{\pm} produced through pp interactions inside the same sources

where GCR protons are accelerated, *e.g.* SNRs, can produce a hard positron component [19]. We recapitulate here the essential formalism of diffusive shock acceleration [16, 17] which yields the spectrum of the accelerated protons. This serves as the source term for calculating the spectrum of the secondary e^\pm .

The phase space density, f_\pm , of secondary e^- and e^+ produced by the primary GCR, both undergoing DSA, is described by the steady state transport equation:

$$u \frac{\partial f_\pm}{\partial x} = \frac{\partial}{\partial x} \left(D \frac{\partial f_\pm}{\partial x} \right) + \frac{1}{3} \frac{du}{dx} p \frac{\partial f_\pm}{\partial p} + q_\pm, \quad (12)$$

where q_\pm is the source term determined by solving an analogous equation for the primary GCR protons. (Ideally we should solve the time-dependent equation, however we do not know the time-dependence of the parameters and can extract only their effective values from observations. This ought to be a good approximation for calculating *ratios* of secondaries to primaries from a large number of sources which are in different stages of evolution.) We consider the usual setup in the rest-frame of the shock front (at $x = 0$) where u_1 (u_2) and n_1 (n_2) denote the upstream (downstream) plasma velocity and density, respectively. The compression ratio of the shock $r = u_1/u_2 = n_2/n_1$ determines the spectral index, $\gamma = 3r/(r-1)$, of the GCR primaries in momentum space (note $\gamma = 2 + \Gamma$). To recover $\gamma \simeq 4.4$ as determined from γ -ray observations (see Table I) we set $r \simeq 3.1$. As noted earlier the theoretical expectation is however $r = 4$.

For $x \neq 0$, Eq. (12) reduces to an ordinary differential equation in x that is easily solved taking into account the spatial dependence of the source term

$$q_\pm^0(x, p) = \begin{cases} q_{\pm,1}^0(p) e^{x u_1/D(p_p)} & \text{for } x < 0, \\ q_{\pm,2}^0(p) & \text{for } x > 0, \end{cases} \quad (13)$$

where the proton momentum p_p should be distinguished from the (smaller) momentum p of the produced secondaries, the two being related through the inelasticity of e^\pm production: $\xi \simeq 1/20$. Assuming $D \propto p$ (Bohm diffusion) in the SNR, the solution to the transport equation (12) across the shock can then be written (see Appendix B):

$$f_\pm = \begin{cases} f_\pm^0 e^{x/d_1} - \frac{q_{\pm,1}^0}{u_1} d_1 \left(\frac{e^{x/d_1} - e^{\xi x/d_1}}{\xi - \xi^2} \right) & \text{for } x < 0, \\ f_\pm^0 + \frac{q_{\pm,2}^0}{u_2} x & \text{for } x > 0, \end{cases} \quad (14)$$

where $d_1 \equiv D/u_1$ is the effective size of the region where e^- and e^+ participate in DSA (see Fig. 4).

The coefficients f_\pm^0 appearing in Eq. (14) satisfy an ordinary differential equation dictated by continuity across the shock front (see Appendix B). This has the solution:

$$f_\pm^0(p) = \gamma \left(\frac{1}{\xi} + r^2 \right) \int_0^p \frac{dp'}{p'} \left(\frac{p'}{p} \right)^\gamma \frac{D(p') q_{\pm,1}(p')}{u_1^2}. \quad (15)$$

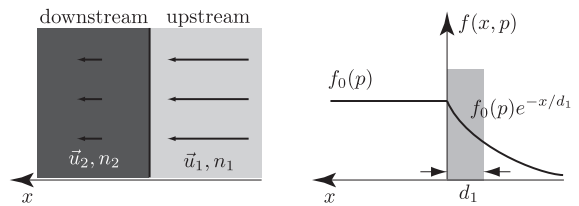


FIG. 4: DSA setup in the rest frame of the shock front. u_1 (u_2) and n_1 (n_2) denote upstream (downstream) plasma velocity and density, respectively. The right panel shows the solution of the transport equation for the primary GCRs. Particles within a distance D/u of the shock front participate in the acceleration process.

Assuming Feynman scaling for the pp interaction, *i.e.* $p d\sigma_{pp}/dp \propto \Sigma_\pm$ we can express the momentum dependence of the source term as

$$q_{\pm,1}(p) = \frac{c n_{\text{gas},1}}{4\pi p^2} \int_p^\infty dp' N_{\text{CR}}(p') \frac{d\sigma_{pp \rightarrow e^\pm + X}}{dp} \\ \simeq \frac{c n_{\text{gas},1}}{4\pi p^2} N_{\text{CR}}(p) \frac{\Sigma_\pm}{\gamma - 2}. \quad (16)$$

The maximum energy of protons is determined from the average maximum γ -ray energy $E_{\text{max}} \simeq 20$ TeV (see Table I) through the inelasticity of the $pp \rightarrow \gamma + X$ process as $\sim 20 \text{ TeV}/0.15 \approx 100 \text{ TeV}$ [38].

We can easily interpret the solution (14) in terms of power laws in momentum. The second term downstream, $(q_2^0/u_2)x$, follows the spectrum of the primary GCRs ($\propto p^{-\gamma}$) and describes the production of secondary e^- and e^+ that are then advected away from the shock front. However, secondaries that are produced within a distance $\sim D/u$ from the shock front are subject to DSA (see Eq. 13 and Fig. 4). The fraction of secondaries that enters the acceleration process is thus given by the ratio of the relevant volumes, *i.e.* $(D/u_1)/(u_2 \tau_{\text{SNR}})$, and the number density injected into the acceleration process is $(1/\xi + r^2) D q_{\pm,1}/u_1^2$. This rises with energy because of the momentum dependence of the diffusion coefficient ($D(p) \propto p$) so the first term downstream in Eq. (14) gets harder: $f_\pm^0(p) \propto p^{-\gamma+1}$.

The injection spectrum R_\pm is obtained by integrating the steady state solution over the volume of the SNR:

$$R_\pm = 4\pi p^2 4\pi \int_0^{u_2 \tau_{\text{SNR}}} dx x^2 f_\pm(x, p). \quad (17)$$

The resulting source spectrum, R_\pm , is thus the sum of two power laws,

$$R_\pm \simeq R_\pm^0 p^{-\gamma+2} \left[1 + \left(\frac{p}{p_{\text{cross}}} \right) \right], \quad (18)$$

where the “cross-over” momentum, p_{cross} , satisfies

$$D(p_{\text{cross}}) = \frac{3}{4} \frac{r u_1^2 \tau_{\text{SNR}}}{\gamma (1/\xi + r^2)}. \quad (19)$$

As has been noted [19], this mechanism is most efficient for *old* SNRs where field amplification by the shock wave is not very effective anymore. We therefore introduce a fudge factor K_B that parameterises the effect of the smaller field amplification on the otherwise Bohm-like diffusion coefficient in the SNR,

$$D(E) = 3.3 \times 10^{22} K_B \left(\frac{B}{\mu\text{G}} \right)^{-1} \left(\frac{E}{\text{GeV}} \right) \text{cm}^2 \text{s}^{-1}. \quad (20)$$

The number of particles entering the acceleration process can of course not exceed the total number of secondaries produced inside the SNR. This effectively caps the growth of the term $D(p')q_{\pm,1}^0(p')/u_1^2$ once $(D/u_1)/(u_2 \tau_{\text{SNR}})$ becomes larger than unity, a relation that defines a characteristic momentum scale p_{break} . We therefore substitute in Eq. (15),

$$\frac{D(p)q_{\pm,1}^0(p)}{u_1^2} \rightarrow \begin{cases} \frac{D(p)q_{\pm,1}^0(p)}{u_1^2} & \text{for } p < p_{\text{break}}, \\ \frac{D(p_{\text{break}})q_{\pm,1}^0(p)}{u_1^2} & \text{for } p > p_{\text{break}}. \end{cases} \quad (21)$$

The source spectrum R_{\pm} thus returns to a $p^{-\gamma}$ dependence around $p = p_{\text{break}}$. At even higher energies the secondary spectrum cuts off at the same E_{cut} as for primary electrons (see sec. III A).

Following Refs. [19, 23], the parameters are chosen to be: $u_1 = 0.5 \times 10^8 \text{cm s}^{-1}$, $n_{\text{gas},1} = 2 \text{cm}^{-3}$, $B = 1 \mu\text{G}$. Choosing $r = 3.1$ to recover $\Gamma = 2.4$ the characteristic momenta p_{cross} and p_{break} turn out to be,

$$p_{\text{cross}} = 427 K_B^{-1} \left(\frac{\tau_{\text{SNR}}}{10^4 \text{yr}} \right) \text{GeV}, \quad (22)$$

$$p_{\text{break}} = 7.7 K_B^{-1} \left(\frac{\tau_{\text{SNR}}}{10^4 \text{yr}} \right) \text{TeV}. \quad (23)$$

What is still missing is the normalization of the injection spectrum, R_{\pm}^0 , in the sources which is proportional to the normalisation of the GCR protons, N_{GCR} , through Eq. (13). Usually a factor $K_{\text{ep}} \simeq 10^{-4} - 10^{-2}$ is introduced to normalize the electron component with respect to the protons; this depends on how particles are injected from the thermal background into the acceleration process and is not reliably calculable from first principles. We can get around this by assuming that the γ -rays detected from known SNRs by HESS are of hadronic origin, as is expected in this framework. Thus we can use the total luminosity of individual sources in γ -rays,

$$Q_{\gamma} = 4\pi d^2 J_{\gamma}, \quad (24)$$

to determine the normalization of the proton component and therefore also the secondary injection rate q_{\pm}^0 .

The compilation of γ ray data on SNRs from HESS, see Table I, suggests an average value $Q_{\gamma}^0 \simeq 5.7 \times 10^{33} \text{s}^{-1} \text{TeV}^{-1}$. We find then for the total spectrum

$$R_{+}^0 = \tau_{\text{SNR}} Q_{+}^0 \simeq \tau_{\text{SNR}} \frac{\Sigma_{+}}{\Sigma_{\gamma}} Q_{\gamma}^0, \quad (25)$$

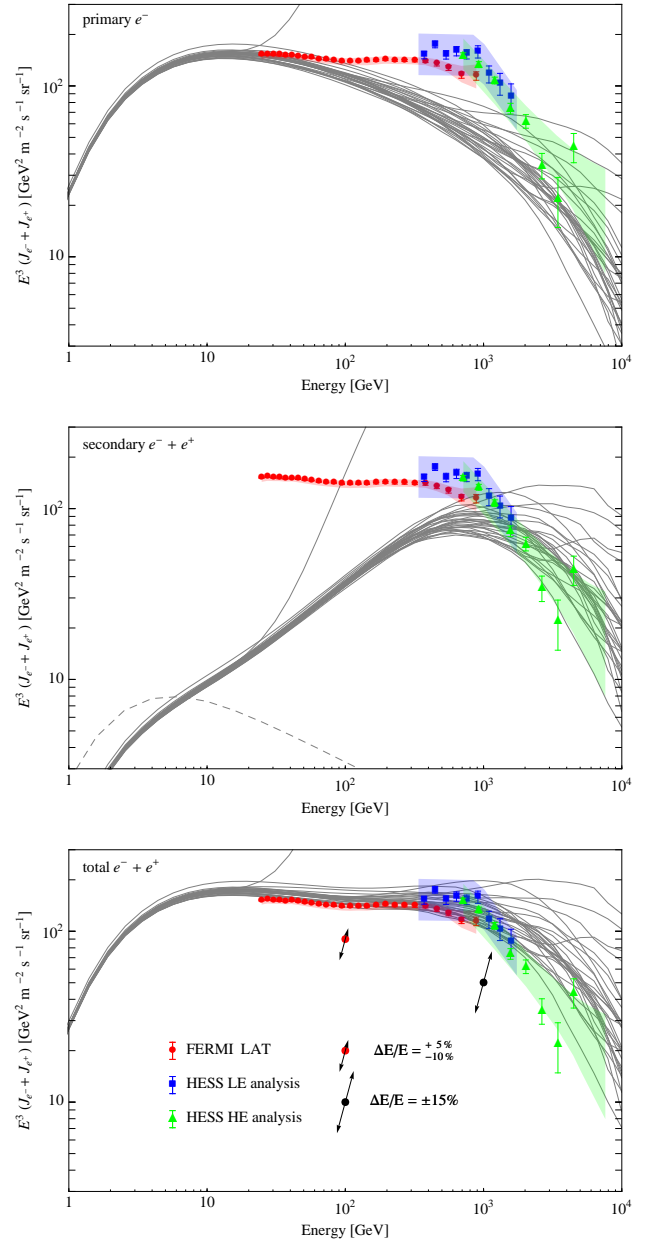


FIG. 5: Predicted spectra of electrons and positrons with data from Fermi LAT [4] (red circles) and HESS [5, 6] (blue squares & green triangles). The diagonal arrows show the energy scale uncertainty. **Top:** Primary electrons after propagation to Earth. **Middle:** Secondary electrons and positrons from cosmic ray interactions, created during propagation (dashed line) and created during acceleration in SNRs (full lines). **Bottom:** The sum of primary and secondary electrons and positrons.

where Σ_{+} (and analogously Σ_{γ}) are defined by Eq. (16), or explicitly

$$R_{+}^0 = 7.4 \times 10^{48} \left(\frac{\tau_{\text{SNR}}}{10^4 \text{yr}} \right) \left(\frac{Q_{\gamma}^0}{5.7 \times 10^{33} \text{s}^{-1} \text{TeV}^{-1}} \right) \text{GeV}^{-1}. \quad (26)$$

Diffusion Model		
D_0	$10^{28} \text{ cm}^2 \text{ s}^{-1}$	} from GCR nuclear secondary-to-primary ratios
δ	0.6	
L	3 kpc	
b	$10^{-16} \text{ GeV}^{-1} \text{ s}^{-1}$	CMB, IBL and \vec{B} energy densities
Source Distribution		
t_{max}	$1 \times 10^8 \text{ yr}$	from $E_{\text{min}} \simeq 3.3 \text{ GeV}$
τ_{SNR}	10^4 yr	from observations
N	3×10^6	from number of observed SNRs
Source Model		
$R_{e^-}^0$	$1.8 \times 10^{50} \text{ GeV}^{-1}$	fit to e^- flux at 10 GeV
Γ	2.4	average γ -ray spectral index
E_{max}	20 TeV	typical γ -ray maximum energy
E_{cut}	20 TeV	DSA theory
R_+^0	$7.4 \times 10^{48} \text{ GeV}^{-1}$	<i>cf.</i> Sec. III C
K_B	15	only free parameter (for fixed Γ)

TABLE II: Summary of parameters used in the Monte Carlo simulation, for an injection spectral index $\Gamma \simeq 2.4$.

In the Monte Carlo code we have explicitly input the experimentally measured pp cross-section which gives a similar normalisation as the estimate presented above assuming Feynman scaling. The normalisation for secondary electrons is computed similarly.

The middle panel of Fig. 5 shows an example of the flux of secondary source e^- and e^+ for 30 “histories” of SNRs in our Galaxy. Clearly this component can potentially match the high energy Fermi LAT and HESS data.

We note that in our model, the contribution from secondary electrons and positrons to the total flux is about twice as large as in ref.[19] where the primary injection spectrum was assumed to be $\propto E^{-2}$, motivated by DSA theory. However this is not consistent with γ -ray observations of SNRs as seen from Table I.

IV. RESULTS

The parameters used in the Monte Carlo are given in Table II. For an assumed injection spectral index Γ , the only free parameter is p_{cross} (*cf.* Eq. (19)) or, equivalently, the factor K_B (*cf.* Eq. (20)) which is determined by fitting the total flux of electrons and positrons to the Fermi LAT and HESS data (see Fig. 5). Adopting $\Gamma = 2.4$, we find good agreement for $K_B \simeq 15$, which corresponds to a cross-over of the primary and (accelerated) secondary components at $p_{\text{cross}} \simeq 28 \text{ GeV}$ and a spectral break at $p_{\text{break}} \simeq 510 \text{ GeV}$ (*cf.* Eqs. (22) and (23)).

We have calculated the χ^2 with respect to the combined Fermi LAT and HESS data for each configuration m of source distances and times, $\{d_i, t_i\}_m$, over all energy bins j . The three best “fits” are shown in Fig. 6 for different values of K_B and for $\Gamma = 2.3, 2.4$ and 2.5 (see Table II). The corresponding predictions for

the e^+ fraction are shown in the bottom panels. These agree reasonably well with the data down to 6 GeV; we would not expect agreement at lower energies since we have neglected convection and reacceleration during interstellar propagation. In fact the PAMELA measurements of the e^+ fraction are systematically lower than previous measurements, *e.g.* AMS-01 or HEAT, and it has been noted that this discrepancy can be resolved by considering charge-sign *dependent* Solar modulation with $\phi_+ = 438 \text{ MV}$ for e^+ and $\phi_- = 2 \text{ MV}$ for e^- [52] (rather than $\phi_+ = \phi_- = 600 \text{ MV}$). This however seems to be at odds with preliminary PAMELA data on the absolute electron flux [50] which *does* show substantial Solar modulation. Accordingly in Fig.6 we have shown the predicted e^+ fraction for both cases; note that this does not affect our predictions for energies above 10 GeV.

Thus our fits to both the PAMELA and the Fermi LAT spectra, including secondary e^+ accelerated in SNRs, provides a consistent picture of current data on cosmic ray e^- and e^+ between a few GeV and tens of TeV. Turning the argument around, since a large fraction of the e^- and e^+ observed in GCR above hundreds of GeV are required to be secondaries in this model, there *must* be a large number of hadronic cosmic ray accelerators in our Galaxy, some of which should be quite nearby.

An independent test of the model is provided by the usual ‘messengers’ of such hadronic acceleration environments, namely γ -rays and neutrinos. Taking the known distribution of SNRs in the Galaxy (see Sec. II) we have calculated the column depth in SNRs in the Galactic disk as seen from Earth,

$$X(\phi') = \int_0^\infty dr' r' g(r(r', \phi'), \phi(r', \phi')), \quad (27)$$

and show this in the top panel of Fig. 7. As expected, the column depth is largest towards the Galactic centre. However, the quantity that is more important for observations is the brightness of sources. We have therefore weighted the integrand in Eq. (27) by $1/r^2$ and this flux weighted column depth is also shown in the top panel of Fig. 7. We note that although the maximum brightness is still expected around the Galactic Centre, the brightness in other directions is smaller by only $\sim 30\%$ because the sources in the closest spiral arms are then dominant (if they are actually there of course).

This is illustrated in the bottom panel of Fig. 7 by an example distribution of SNRs from the Monte Carlo simulation, denoted by circles. The position of the circle denotes the Galactic longitude and the radius is proportional to the brightness in units of the Crab Nebula, *i.e.* an integrated flux of $(1.98 \pm 0.08) \times 10^{-11} \text{ cm}^{-2} \text{ s}^{-1}$ above 1 TeV [58]. For a source of luminosity of $Q_\gamma^0 = 5.7 \times 10^{33} \text{ TeV}^{-1} \text{ s}^{-1}$ (see Table I) at distance d , the in-

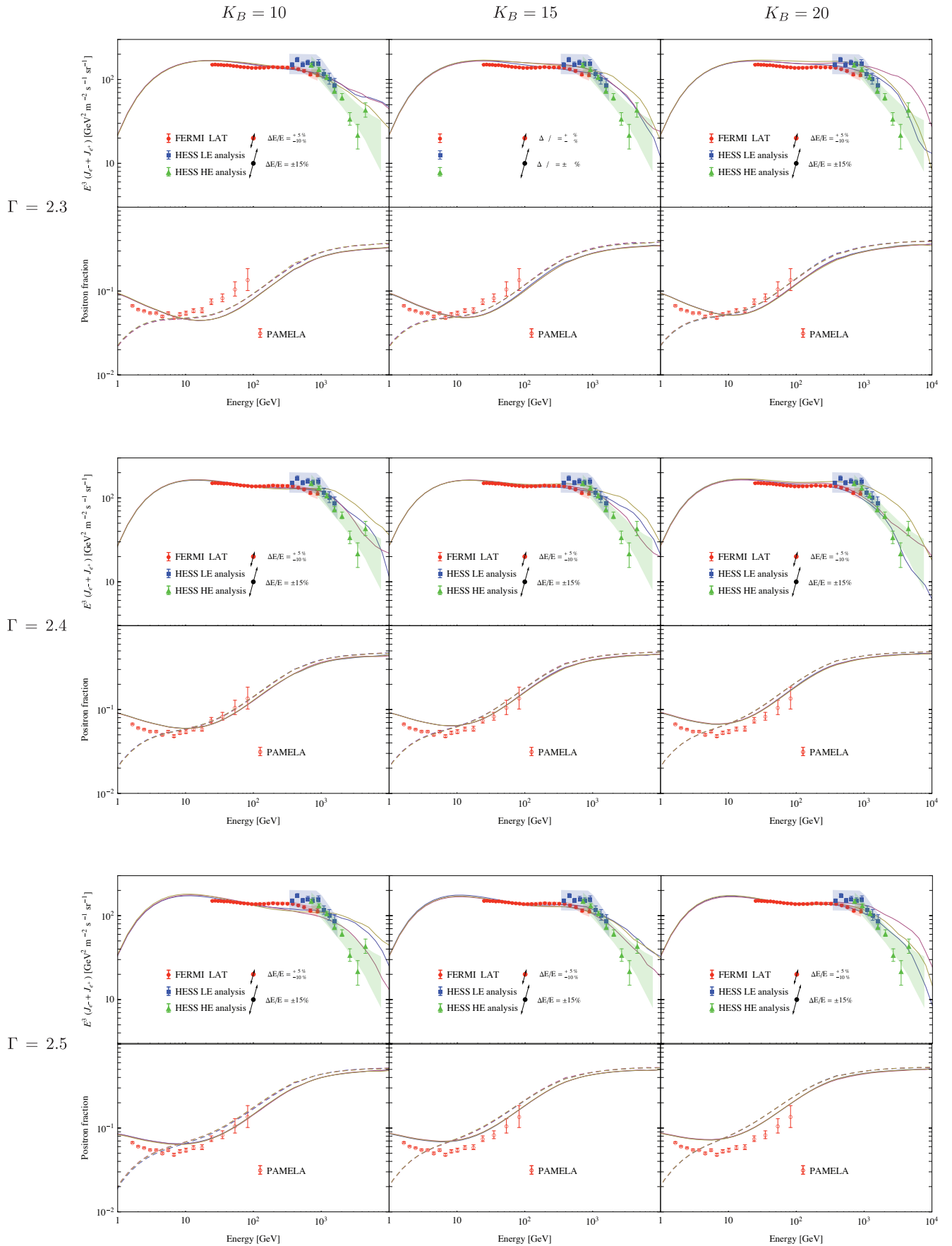


FIG. 6: The three best fits (out of 30 source “histories”) to the total spectrum of electrons and positrons measured by Fermi LAT [4] (red circles) and HESS [5, 6] (blue squares & green triangles), and the corresponding prediction for the positron fraction for different values of Γ and K_B , for both charge-sign independent (full line) and charge-sign dependent (dashed line) Solar modulation (see text for details). The PAMELA data [1] is shown for comparison (open red circles).

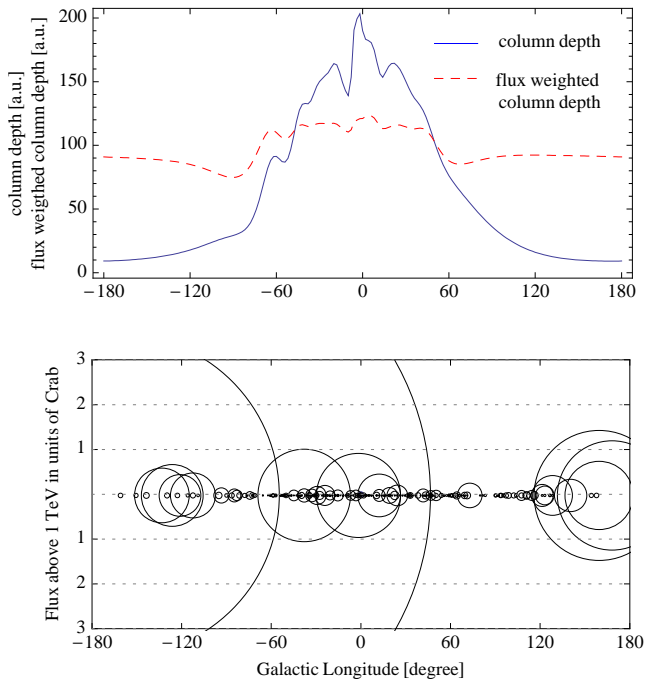


FIG. 7: **Top:** The column depth and flux weighted column depth of the SNR density in the Galactic plane. **Bottom:** Example of a distribution of SNRs in γ -rays/neutrinos from the Monte Carlo simulation. The position of a circle denotes the Galactic longitude of the source and the radius is proportional to the brightness in units of the Crab nebula. One source whose circle exceeds the vertical scale is ~ 500 pc from Earth and has a total integrated flux above 1 TeV of ~ 6 times the Crab Nebula.

egrated flux above 1 TeV is,

$$F_{\gamma}(> 1\text{TeV}) = \frac{1}{4\pi d^2} \int_{1\text{TeV}} dE Q_{\gamma} \\ \simeq 8.5 \times 10^{-12} \left(\frac{d}{2\text{kpc}} \right)^{-2} \text{cm}^{-2} \text{s}^{-1}, \quad (28)$$

i.e. about 40 % of the Crab Nebula flux at $d = 2$ kpc. It is seen that although most of the sources are clustered towards the Galactic centre, there are several bright sources at large longitudes as well. We find typically ~ 3 sources brighter than the Crab (or ~ 7 brighter than 50 % Crab).

The adopted distribution of SNRs (Sec. II) and the average luminosity per source determined from a compilation of known sources (Table I) thus leads to the prediction of several nearby SNRs with fluxes of the order of the Crab Nebula. Note, however, that close sources could be rather extended and thus have escaped detection by HESS in one of its surveys of the Milky Way [44, 60, 61]. For example, a diameter of ~ 50 pc which is a typical value for a very old SNR, corresponds to 1.5° at 2 kpc.

Extended γ -ray luminous SNRs can however be detected by MILAGRO [59] with its larger field of view. A survey in Galactic longitude $l \in [30^\circ, 220^\circ]$ and latitude $b \in [-10^\circ, 10^\circ]$ has revealed 6 new sources at a median

energy of 20 TeV, several of which are spatially extended. The flux from a SNR of the above luminosity at $d = 2$ kpc is $Q_{\gamma}^0/(4\pi d^2) \simeq 1.2 \times 10^{-11} \text{TeV}^{-1} \text{cm}^{-2} \text{s}^{-1}$ at 1 TeV. Scaled with a spectral index of 2.4 to 20 TeV, this gives $Q_{\gamma}^0/(4\pi d^2) 20^{-2.4} \simeq 9.0 \times 10^{-15} \text{TeV}^{-1} \text{cm}^{-2} \text{s}^{-1}$ which is in the range of the unidentified MILAGRO sources [59]. We note that the MILAGRO source MGRO J1908+06 was recently confirmed by HESS [62], though with a smaller angular extent of $\sim 0.7^\circ$. However, correlating unidentified MILAGRO sources with the FERMI BSL list [63, 64] seems to favour associations with pulsars, although several new unidentified extended sources have also been found.

Hadronic sources of cosmic rays should also be visible by their neutrino emission. On general grounds, the neutrino luminosity (from π^\pm decay) can be directly related to the γ -ray luminosity (from π^0 decay) and should be of the same order of magnitude since pp interactions produce π^+ , π^0 and π^- in roughly equal numbers. Each of the three neutrinos produced in the decay chains $\pi^+ \rightarrow \mu^+ \nu_{\mu} \rightarrow e^+ \nu_e \bar{\nu}_{\mu} \nu_{\mu}$ and $\pi^- \rightarrow \mu^- \bar{\nu}_{\mu} \rightarrow e^- \bar{\nu}_e \nu_{\mu} \bar{\nu}_{\mu}$ carries about half of the energy of each photon produced in the decay $\pi^0 \rightarrow \gamma\gamma$. Hence, the ratio of neutrinos to photons produced on average is $\sim 3 : 1$ and the total neutrino luminosity is

$$Q_{\text{all } \nu}(E_{\nu}) \simeq 6Q_{\gamma}(2E_{\nu}) \\ \simeq 6 \times 2^{-\Gamma} Q_{\gamma}^0 \left(\frac{E_{\nu}}{\text{TeV}} \right)^{-\Gamma}. \quad (29)$$

Presently the largest cosmic neutrino detector is the IceCube observatory [65] under construction at the South Pole. IceCube observes high energy neutrinos via their interactions with nucleons in the vicinity of the detector and subsequent Čerenkov light emission of energetic charged particles in the transparent glacial ice. The most important signal for neutrino astronomy is the Čerenkov radiation by muons produced via charged current interactions of muon neutrinos. Since the muon inherits the large boost of the initial neutrino the point source resolution is $\sim 1^\circ$. The large background signal of atmospheric muons is efficiently reduced for upward-going muons, *i.e.* neutrino sources which are somewhat below the horizon. Hence, IceCube is mainly sensitive to neutrino point sources in the northern sky, which excludes SNRs in the direction of the Galactic centre.

Neutrino emission associated with galactic TeV γ -ray sources has been investigated by many authors [66, 67, 68, 69, 70, 71] including also the HESS sources used in our analysis. In particular, Ref. [67] investigates the prospects of neutrino detection for the SNRs HESS J0852.0-463, J1713-381, J1804-216, J1834-087 (see Table I) in the proposed KM3NeT detector in the Mediterranean which will see the Galactic centre region. The muon neutrino rate is expected to be a few events per year for such sources.

Due to flavour oscillations of neutrinos with large mixing angles, the initial flavour composition $Q_{\nu_e} : Q_{\nu_{\mu}} :$

$Q_{\nu_\tau} \simeq 1 : 2 : 0$ from pion decay is expected to become $\sim 1 : 1 : 1$ at Earth. The TeV muon neutrino point flux from a hadronic γ -ray source located at a distance d and with a power-law index $\Gamma \simeq 2.4$ is thus $F_{\nu_\mu}(> 1 \text{ TeV}) \simeq 2^{1-\Gamma} F_\gamma(> 1 \text{ TeV})$, hence

$$F_{\nu_\mu}(> 1 \text{ TeV}) \simeq 3.2 \times 10^{-12} \left(\frac{d}{2 \text{ kpc}} \right)^{-2} \text{ cm}^{-2} \text{ s}^{-1}. \quad (30)$$

This should be compared to the results of searches for neutrino point sources in the northern sky, in particular the close-by SNR Cassiopeia A (see Table I), using data taken with AMANDA-II (the predecessor of IceCube) during 2000–2006 [72] and, more recently, with the first 22 strings of IceCube during 2007–08 [73]. The average 90% C.L. upper limit on the integrated ν_μ flux in the energy range 3 TeV to 3 PeV is [73]

$$F_{\nu_\mu} \leq 4.7 \times 10^{-12} \text{ cm}^{-2} \text{ s}^{-1}, \quad (31)$$

i.e. well above the flux of $\sim 7 \times 10^{-13} \text{ cm}^{-2} \text{ s}^{-1}$ expected from a SNR at 2 kpc, assuming $\Gamma = 2.4$.

The full 80 string configuration of IceCube thus has excellent prospects to identify these SNRs. A point source in the northern sky with an E^{-2} muon neutrino flux,

$$F_{\nu_\mu} \simeq 7.2 \times 10^{-12} \text{ cm}^{-2} \text{ s}^{-1}, \quad (32)$$

in the TeV-PeV range can be detected with a 5σ significance after three years of observation. This does depend somewhat on the spectral index and energy cut-off, since the signal (after “level 2 cuts”) peaks at an energy of $\sim 10 \text{ TeV}$ [65]. As mentioned previously, our analysis predicts on average ~ 3 nearby γ -ray sources stronger than Crab with corresponding muon neutrino fluxes larger than $\sim 7 \times 10^{-12} \text{ cm}^{-2} \text{ s}^{-1}$. Note that although the Galactic centre is not in the field of view of IceCube, SNRs following the spiral arm structure of the Galaxy are expected to be detected also in the Galactic anti-centre direction, as seen in the example distribution shown in the bottom panel of Fig. 7.

V. SUMMARY

Supernova remnants have long been suspected to be the sources of Galactic cosmic rays. We have discussed a recent proposal [19] that proton-proton interactions in the shocks of SNRs followed by the diffusive shock acceleration of the secondary positrons produced can flatten the spectrum of the secondaries relative to that of the primaries. These hard spectra may be the origin of the recently observed cosmic ray “excesses” — both the e^+ fraction observed by PAMELA [1] and the $e^- + e^+$ flux measured by Fermi LAT [4] and HESS [5, 6].

We have investigated how γ -ray emission of SNRs — assumed to be of the same hadronic origin as the positrons

— together with cosmic ray data, constrain the acceleration of positrons. We have accounted for the spatial and temporal discreteness of SNRs via a Monte Carlo exercise, drawing samples from a realistic galactic distribution with the observed SN rate. For the diffusion parameters we have adopted standard values derived from cosmic ray nuclear-to-primary ratios, as well as the energy densities of galactic radiation and magnetic fields.

We have compiled a list of all γ -ray emitting SNRs observed by HESS and determined the mean value of the flux, which fixes the hadronic interaction rate in the SNR. Low energy data from PAMELA on the absolute e^- flux was used to normalize the primary flux of e^- . The contribution from accelerated e^+ was then found by fitting the $e^- + e^+$ flux to Fermi LAT and HESS data, adjusting the (only) free parameter K_B which determines the diffusion rate near SNR shocks.

The spectra of e^+ and e^- thus derived agrees well with the e^+ fraction observed by PAMELA in the range 5 – 100 GeV. The apparent deficit at lower energies can be attributed to convection and diffusive reacceleration of primary electrons that become important at these energies and were neglected in our analysis. The flux of e^+ and e^- becomes dominated by the accelerated secondary component at high energies; the corresponding e^+ fraction levels out at ~ 0.4 , reflecting the relative multiplicity of e^+ and e^- produced by p-p interactions.

We note that although the value of ~ 10 – 20 found here for K_B differs from the value of ~ 40 we had found earlier from our analysis of the titanium-to-iron (Ti/Fe) ratio in cosmic rays [24], the latter determination is subject to

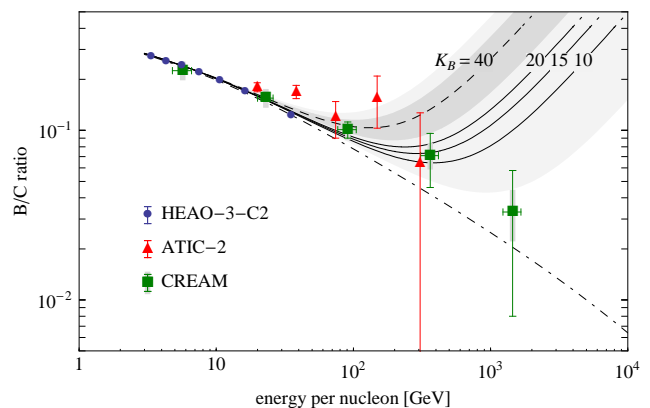


FIG. 8: The B/C ratio in cosmic rays along with model predictions (after Ref. [24]) — the leaky box model with production of secondaries during propagation only (dot-dashed line), and including production and acceleration of secondaries in a nearby SNR (solid lines) for values of the diffusion coefficient near the shock wave which best fit the e^\pm spectrum (see Fig.6). The dashed line corresponds to the value of the diffusion co-efficient required to fit the ATIC-2 data on Ti/Fe (from Ref.[24]), along with the 1σ and 2σ error bands. The data points are from HEAO-3-C2 (circles) [74], ATIC-2 (triangles) [75] and CREAM (squares) [76].

large uncertainties due to poor experimental statistics at high energies. This affects our previous prediction [24] for the boron-to-carbon (B/C) ratio and we show in Fig. 8 the corresponding 1σ and 2σ error bands, along with the prediction taking $K_B \sim 10 - 20$ as indicated by our new fits to the e^\pm spectrum. The predicted upturn at high energies will soon be tested by PAMELA and AMS-02.

To be consistent with our overall framework the γ -rays observed from SNRs have been assumed to be of hadronic origin. The known spatial distribution of SNRs then implies (on average) several nearby sources with a γ -ray flux comparable to the Crab. We have speculated that some unidentified MILAGRO sources [59] might correspond to such old SNRs. Moreover, the same hadronic processes in SNRs will inevitably produce high energy neutrinos which can be detected in cubic-km telescopes such as IceCube [65]. The neutrino luminosity can be directly related to the γ -rays and is not connected to the hypothetical acceleration of e^+ and e^- in the sources as in our present model. Nevertheless, similarly to the previous argument, we expect on average a few nearby sources, some of which may also lie within the field of view of IceCube and can thus be detected with high statistical significance after three years of data taking.

While our calculational framework is based on first-order Fermi acceleration by SNR shock waves, we have noted that in detail the observations do not fit the theoretical expectations, *e.g.*, the shock compression ratio inferred from the observed γ -ray spectrum ($\sim E^{-2.4}$) is 3.1 rather than 4 as is expected for a strong shock [16]. Going beyond the test particle approximation, the generic expectation in such a process is for particle spectra which are much flatter than those observed ($\sim E^{-1.4}$ and slightly *concave*), when the back reaction of the cosmic rays on the shock is taken into account [17]. By contrast, the observed radio spectrum of Cassiopeia A is slightly *convex* and this, as well as the morphology and time evolution of radio emission from such young SNRs, can be well explained in terms of *second-order* Fermi acceleration by plasma turbulence behind the shock wave [77]. Moreover the observed spatial correlation between the γ -ray emission and the hard X-ray emission from some SNRs argues for a leptonic rather than hadronic origin and further observations are necessary to resolve this issue [78]. It has been argued that cosmic ray protons and nuclei may well have different sources (*e.g.* “super-bubbles” formed by multiple supernovae) than the cosmic ray electrons [79]. The additional predictions made in this paper concerning the visibility of hadronic accelerators in γ -rays and neutrinos, tied to the expectations for the fluxes of the accelerated *secondary* positrons in cosmic rays, will hopefully enable further consistency tests of the SNR origin hypothesis for galactic cosmic rays.

Acknowledgements

We thank Tyce DeYoung, Pascuale Serpico and Andrew Strong for useful discussions. This work was supported by the EU Marie Curie Network “UniverseNet” (HPRN-CT-2006-035863) and STFC (PP/D00036X/1).

APPENDIX A: GREEN’S FUNCTION OF DIFFUSION EQUATION

We solve Eq. (1) for a halo of extent $\pm L$ in z direction, neglecting the boundaries in the radial direction. The Green’s function for the flux of electrons from a source at \vec{r} that went off a time t ago with a spectrum $Q(E)$, is:

$$\begin{aligned} G_{\text{disk}}(E, \vec{r}, t) &= \sum_{n=-\infty}^{\infty} \frac{1}{(\pi \ell^2)^{\frac{3}{2}}} e^{-\vec{r}_n^2/\ell^2} Q\left(\frac{E}{1-b_0Et}\right) \left(\frac{1}{1-b_0Et}\right)^2 \\ &= \frac{1}{\pi \ell^2} e^{-\vec{r}_{\parallel}^2/\ell^2} \frac{QE}{(1-b_0Et)^3} \frac{1}{\ell_{\text{cr}}} \chi(z/\ell_{\text{cr}}, \ell/\ell_{\text{cr}}), \end{aligned} \quad (\text{A1})$$

where

$$\chi(\hat{z}, \hat{\ell}) \equiv \frac{1}{\sqrt{\pi} \hat{\ell}} \sum_{n=-\infty}^{\infty} e^{-\hat{z}_n^2/\hat{\ell}^2}, \quad (\text{A2})$$

and the diffusion length ℓ is defined as

$$\begin{aligned} \ell^2 &= 4 \int_E^{E/(1-b(E)t)} dE' \frac{D(E')}{b(E')} \\ &= \frac{4D_0}{b_0(1-\delta)} \left[E^{\delta-1} - \left(\frac{E}{1-b_0Et}\right)^{\delta-1} \right], \end{aligned} \quad (\text{A3})$$

with $\ell_{\text{cr}} \equiv 4L/\pi$. If we neglect the spatial extent of the disk and set $z = 0$, the function $\chi(0, \hat{\ell})$ is approximately:

$$\chi(0, \hat{\ell}) \simeq \begin{cases} \frac{4}{\pi} e^{-\hat{\ell}^2} & \text{for } \hat{\ell} \gg \frac{\pi}{4}, \\ \frac{1}{\sqrt{\pi} \hat{\ell}} & \text{for } \hat{\ell} \ll \frac{\pi}{4}. \end{cases} \quad (\text{A4})$$

In practice both limits can be connected at $\hat{\ell} \simeq 0.66$ such that the approximated $\chi(0, \hat{\ell})$ has a relative error of at most 0.5%. We motivate the choice of the parameters of our diffusion model from an analysis of nuclear secondary-to-primary ratios [57]: $D_0 = 10^{28} \text{ cm}^2 \text{ s}^{-1}$, $\delta = 0.6$, $L = 3 \text{ kpc}$, and from the Galactic magnetic field and interstellar radiation fields [28]: $b_0 = 10^{-16} \text{ GeV}^{-1} \text{ s}^{-1}$.

APPENDIX B: BOUNDARY CONDITIONS OF DSA

The solution (14) of Eq. 12 satisfies

$$\lim_{x \rightarrow -\infty} f_{\pm} = 0, \quad \lim_{x \rightarrow -\infty} \frac{\partial f_{\pm}}{\partial x} = 0 \quad \text{and} \quad \left| \lim_{x \rightarrow \infty} f_{\pm} \right| < \infty, \quad (\text{B1})$$

Continuity at the shock front $x = 0$ requires:

$$D \frac{\partial f_{\pm}}{\partial x} \Big|_{x=0^-} - D \frac{\partial f_{\pm}}{\partial x} \Big|_{x=0^+} = \frac{1}{3}(u_2 - u_1)p \frac{\partial f_{\pm}^0}{\partial p}, \quad (\text{B2})$$

yielding the differential equation,

$$p \frac{\partial f_{\pm}^0}{\partial p} = -\gamma f_{\pm}^0 + \gamma \left(\frac{1}{\xi} + r^2 \right) \frac{Dq_1^0}{u_1^2}. \quad (\text{B3})$$

This is readily integrated with boundary condition $f_{\pm}^0(0) = 0$ and yields the p dependence in Eq. (15).

-
- [1] O. Adriani *et al.*, Nature **458**, 607 (2009).
 [2] I. V. Moskalenko & A. W. Strong, Astrophys. J. **493**, 694 (1998).
 [3] P. D. Serpico, Phys. Rev. D **79**, 021302(R) (2009).
 [4] A. A. Abdo *et al.*, Phys. Rev. Lett. **102**, 181101 (2009).
 [5] F. Aharonian *et al.*, Phys. Rev. Lett. **101**, 261104 (2008).
 [6] F. Aharonian *et al.*, arXiv:0905.0105 [astro-ph.HE].
 [7] J. Chang *et al.*, Nature **456**, 362 (2008).
 [8] D. Grasso *et al.*, Astropart. Phys. **32**, 140 (2009).
 [9] L. Bergstrom, arXiv:0903.4849 [hep-ph].
 [10] O. Adriani *et al.*, Phys. Rev. Lett. **102**, 051101 (2009).
 [11] G. Bertone, M. Cirelli, A. Strumia and M. Taoso, JCAP **0903**, 009 (2009).
 [12] M. Cirelli and P. Panci, Nucl. Phys. B **821**, 399 (2009).
 [13] F. A. Aharonian, A. M. Atoyan and H. J. Voelk, Astron. Astrophys. **294**, L41(1995).
 [14] D. Hooper, P. Blasi and P. D. Serpico, JCAP **0901**, 025 (2009).
 [15] V. L. Ginzburg, V. A. Dogiel, V. S. Berezhinsky, S. V. Bulanov and V. S. Ptuskin, "Astrophysics of cosmic rays," (Amsterdam: North-Holland, 1990) 534 p.
 [16] R. Blandford & D. Eichler, Phys. Rept. **154**, 1 (1987).
 [17] M. Malkov & L. Drury, Rept. Prog. Phys. **64**, 429 (2001).
 [18] S. P. Reynolds, Annu. Rev. Astron. Astrophys. **46**, 89 (2008).
 [19] P. Blasi, Phys. Rev. Lett. **103**, 051104 (2009).
 [20] D. Eichler, Astrophys. J. **237**, 809 (1980).
 [21] R. Cowsik, Astrophys. J. **241**, 1195 (1980).
 [22] Y. Fujita, K. Kohri, R. Yamazaki and K. Ioka, Phys. Rev. D **80**, 063003 (2009).
 [23] P. Blasi and P. D. Serpico, Phys. Rev. Lett. **103**, 081103 (2009).
 [24] P. Mertsch and S. Sarkar, Phys. Rev. Lett. **103**, 081104 (2009).
 [25] <http://ams.cern.ch/>.
 [26] R. Cowsik and M. A. Lee, Astrophys. J. **228**, 297 (1979).
 [27] M. Pohl and J. A. Esposito, Astrophys. J. **507**, 327 (1998).
 [28] T. Kobayashi, Y. Komori, K. Yoshida and J. Nishimura, Astrophys. J. **601**, 340 (2004).
 [29] R. Cowsik and B. Burch, arXiv:0908.3494 [astro-ph.CO].
 [30] S. Swordy, Proc. 28th International Cosmic Ray Conference, Tsukuba, ed. T. Kajita *et al.* (Tokyo: Universal Academy Press, 2003) p.1989.
 [31] N. J. Shaviv, E. Nakar and T. Piran, Phys. Rev. Lett. **103**, 111302 (2009).
 [32] G. L. Case and D. Bhattacharya, Astrophys. J. **504**, 761 (1998).
 [33] J. P. Vallée, Astron. J. **130**, 569 (2005).
 [34] F. Aharonian *et al.*, Astron. Astrophys. **437**, L7 (2005).
 [35] F. Aharonian *et al.*, AIP Conf. Proc. **1085**, 332 (2009).
 [36] F. Aharonian *et al.*, Astron. Astrophys. **486**, 829 (2008).
 [37] F. Aharonian *et al.*, Astron. Astrophys. **449**, 223 (2006).
 [38] F. Aharonian *et al.*, Astron. Astrophys. **464**, 235 (2007).
 [39] F. Aharonian *et al.*, Astron. Astrophys. **490**, 685 (2008).
 [40] F. Aharonian *et al.*, Astron. Astrophys. **477**, 353 (2008).
 [41] W. W. Tian, D. A. Leahy, M. Haverkorn and B. Jiang, Astrophys. J. **679**, L85 (2008).
 [42] F. Aharonian *et al.*, Astron. Astrophys. **481**, 401 (2008).
 [43] M. Fatuzzo, F. Melia and R. M. Crocker, arXiv:astro-ph/0602330.
 [44] F. Aharonian *et al.*, Astrophys. J. **636**, 777 (2006).
 [45] J. Albert *et al.*, Astrophys. J. **664**, L87 (2007).
 [46] J. Albert *et al.*, Astron. Astrophys. **474**, 937 (2007).
 [47] F. Aharonian *et al.*, Astron. Astrophys. **370**, 112 (2001).
 [48] A. Fiasson, J. A. Hinton, Y. Gallant, A. Marcowith, O. Reimer and G. Rowell, Proc. 30th International Cosmic Ray Conference, Merida, ed. T. Caballero *et al.* (Mexico City: Universidad Nacional Autonoma de Mexico, 2007).
 [49] <http://www.mpi-hd.mpg.de/hfm/HESS/pages/home/sources/>.
 [50] E. Mocchiutti, Talk at 2nd Roma Intern. Conf. on Astroparticle Physics, Rome, 13-15 May 2009.
 [51] L. J. Gleeson and W. I. Axford, Astrophys. J. **154**, 1011 (1968).
 [52] H. Gast and S. Schael, Proc. 31st International Cosmic Ray Conference, Lodz, 2009.
 [53] Y. Shikaze *et al.*, Astropart. Phys. **28**, 154 (2007).
 [54] T. Kamae, N. Karlsson, T. Mizuno, T. Abe and T. Koi, Astrophys. J. **647**, 692 (2006) [Erratum-ibid. **662**, 779 (2007)].
 [55] T. Delahaye, F. Donato, N. Fornengo, J. Lavalle, R. Lineros, P. Salati and R. Taillet, Astron. Astrophys. **501**, 821 (2009).
 [56] L. Stawarz, V. Petrosian and R. D. Blandford, arXiv:0908.1094 [astro-ph.GA].
 [57] A. W. Strong, I. V. Moskalenko and V. S. Ptuskin, Ann. Rev. Nucl. Part. Sci. **57**, 285 (2007).
 [58] F. Aharonian *et al.*, Astron. Astrophys. **425**, L13 (2004).
 [59] A. A. Abdo *et al.*, Astrophys. J. **664**, L91 (2007).
 [60] R. C. G. Chaves, E. de Ona Wilhemi and S. Hoppe, AIP Conf. Proc. **1085**, 219 (2009).
 [61] R. C. G. Chaves *et al.*, arXiv:0907.0768 [astro-ph.HE].
 [62] E. de Ona Wilhelmi, A. Djannati and M. Renaud, AIP Conf. Proc. **1085**, 273 (2009).
 [63] A. A. Abdo *et al.*, Astrophys. J. **700**, L127 (2009).
 [64] A. A. Abdo *et al.*, Astrophys. J. Suppl. **183**, 46 (2009).
 [65] J. Ahrens *et al.*, Astropart. Phys. **20**, 507 (2004).
 [66] L. Anchordoqui, F. Halzen, T. Montaruli and A. O'Murchadha, Phys. Rev. D **76** (2007) 067301 [Erratum-ibid. D **77** (2008) 069906].

- [67] M. D. Kistler and J. F. Beacom, Phys. Rev. D **74**, 063007 (2006).
- [68] J. F. Beacom and M. D. Kistler, Phys. Rev. D **75**, 083001 (2007).
- [69] F. Halzen and A. O'Murchadha, Phys. Rev. D **76**, 123003 (2007).
- [70] F. Halzen, A. Kappes and A. O'Murchadha, Phys. Rev. D **78**, 063004 (2008).
- [71] M. C. Gonzalez-Garcia, F. Halzen and S. Mohapatra, Astropart. Phys. **31**, 437 (2009).
- [72] R. Abbasi *et al.*, Phys. Rev. D **79**, 062001 (2009).
- [73] R. Abbasi *et al.*, Astrophys. J. **701**, L47 (2009).
- [74] J. Engelmann *et al.*, Astron. Astrophys. **233**, 96 (1990).
- [75] A. D. Panov *et al.*, arXiv:0707.4415
- [76] H. S. Ahn *et al.*, Astropart. Phys. **30**, 133 (2008).
- [77] R. Cowsik and S. Sarkar, Mon. Not. R. Astron. Soc. **207**, 745 (1984).
- [78] M. Pohl *et al.*, arXiv:0810.0673 [astro-ph].
- [79] Y. Butt, Nature, **460**, 701 (2009).